Garcia Andres J. (Orcid ID: 0000-0001-6602-2518)

Article I. Title

Impact of Adhesive Area on Cellular Traction Force and Spread Area

Article II. Authors

Elijah N. Holland[1, 2, ‡], Deborah Lobaccaro[1, 4, ‡], Jianping Fu[5], and Andrés J. García[1, 3*]

[1]Petit Institute for Bioengineering and Bioscience, Georgia Institute of Technology, Atlanta, GA, USA

[2]School of Chemical and Biomolecular Engineering, Georgia Institute of Technology, Atlanta, GA, USA

[3]Woodruff School of Mechanical Engineering, Georgia Institute of Technology, Atlanta, GA, USA.

[4]Coulter Department of Biomedical Engineering, Georgia Institute of Technology, Atlanta, GA, USA.

[5]Department of Mechanical Engineering, Department of Biomedical Engineering, Department of Cell & Developmental Biology, University of Michigan, Ann Arbor, MI, USA.

[‡]co-first authors, * corresponding author: andres.garcia@me.gatech.edu

This is the author manuscript accepted for publication and has undergone full peer review but has not been through the copyediting, typesetting, pagination and proofreading process, which may lead to differences between this version and the Version of Record. Please cite this article as doi: 10.1002/jbm.a.37518

Article III. Abstract

Cells integrate endogenous and exogenous mechanical forces to sense and respond to environmental signals. In particular, cell-generated microscale traction forces regulate cellular functions and impact macroscale tissue function and development. Many groups have developed tools for measuring cellular traction forces, including microfabricated post array detectors (mPADs). mPADs are a powerful tool that provides direct traction force measurements through imaging post deflections and utilizing Bernoulli-Euler beam theory. In this technical note, we investigated how mPADs presenting two different top surface areas but similar effective stiffness influence cellular spread area and traction forces for murine embryonic fibroblasts and human mesenchymal stromal cells. When focal adhesion size was restricted via mPAD top surface area, we observed a decrease in both cell spread area and cell traction forces as the mPAD top surface area decreased, but the traction force-cell area linear relationship was maintained, which is indicative of cell contractility. We conclude that the mPAD top surface area is an important parameter to consider when utilizing mPADs to measure cellular traction forces. Furthermore, the slope of the traction force-cell area linear relationship provides a useful metric to characterize cell contractility on mPADs.

Article IV. Keywords

Micropost, Force, Cell Area, Focal Adhesions, Effective Stiffness

Article V. Introduction

Mechanical forces influence many of the body's dynamic processes from embryonic development to wound healing [1, 2]. As the recognition of the importance of these mechanical cues has grown, many research groups have developed methods to characterize the mechanical properties of the extracellular matrix (ECM) and adherent cells [3-5]. Techniques for measuring cellular forces include the spinning disk apparatus [6], which provides a quantifiable measurement of cell adhesion strength, to the molecular tension probe which utilizes a linker, fluorophore, and quencher to infer cell-generated forces at the piconewton level [7]. 2D traction force microscopy (TFM) is used to measure cellular traction forces exerted by cells on a 2D surface. Traditionally, 2D TFM is performed with deformable continuous substrates. Microfabricated post array detectors (mPADs) provide a powerful tool for 2D cellular traction force measurements [8, 9]. mPADs are arrays of micron-sized posts positioned in a repeating hexagonal or square lattice [3, 8]. They can be fabricated from different materials such as silicon or polydimethylsiloxane (PDMS). After the microposts have been functionalized, typically through physically absorbing ECM proteins to the micropost tops, cells can be seeded on top of the microposts. Lateral deflections of the posts due to traction forces exerted by cells can be monitored through microscopy. Forces can then be calculated from the post deflections using the Bernoulli-Euler beam theory. Unlike other platforms to measure traction forces such as continuous substrates embedded with fluorescent beads in TFM, in mPADs, each post moves independently of another, and unlike molecular tension probes, mPADs provide force direction [7]. A limitation of the mPAD platform is the discrete presentation of adhesive ligands at the post tops. This restricts the size of adhesive surfaces available for cells to develop focal adhesions (FA), which are clusters of structural and signaling proteins that anchor

the cell's actomyosin cytoskeleton to the ECM. Whereas smaller post top areas provide more resolution in a cellular force vector map, this further restricts the size of which a FA can grow.

In this study, we investigated the effect of micropost top surface area on cell spread area and traction forces. We used two different micropost array designs, which had the same effective stiffness but different micropost top surface areas. We determined that by reducing post top surface area while keeping mPAD effective stiffness constant, reductions in cell area and traction forces were observed with decreasing micropost top surface area; however, the traction force-cell area linear relationship, which is indicative of cell contractility, was maintained with different micropost top surface areas.

Article VI. Materials and Methods

Cells and Reagents

eGFP-vinculin mouse embryonic fibroblasts (MEFs) were generated by transducing vinculin-null MEFs with retroviral constructs for eGFP-vinculin and sorted by flow cytometry for eGFP expression [10]. Cells were maintained in DMEM containing L-glutamine (Gibco), 10% fetal bovine serum (ATCC), 1% sodium pyruvate (Corning), and 1% penicillin-streptomycin (Corning). Human mesenchymal stromal cells (hMSCs) were acquired from the NIH Resource Center at Texas A&M University (TAMU; College Station, TX). Cells were obtained from healthy willing participants via bone marrow aspirate under IRB-approved protocols and isolated by plastic adherence. Each cell product was certified as hMSCs in accordance with ISCT standards [11] by surface marker and differentiation characterization by the manufacturer. hMSCs were cultured in αMEM (Gibco), 16.5% MSC qualified FBS (Gibco), 2-4 mM of L-glutamine

(Corning), 100 U/mL of penicillin (Corning), 100 µg/mL streptomycin (Corning). Cell Tracker Green CMFDA Dye (ThermoFisher) was used to stain the hMSCs.

mPAD Fabrication

mPADs were fabricated using PDMS (Dow) replica molding from silicon masters [12]. To make negative molds, 1:10 PDMS prepolymer was cast on the desired silicon masters in a foil-lined dish. The PDMS was baked at 110°C for 1 hour. The negative molds were carefully peeled from the masters. Excess PDMS was trimmed from the negative molds, then they were exposed to an oxygen plasma for 5 seconds (Plasma-Preen; Terra Universal) and silanized for 4 hours under vacuum with 1-2 drops of trichloro(1*H*,1*H*,2*H*,2*H*-perfluorooctyl)silane (Sigma–Aldrich). A 1:10 PDMS prepolymer droplet was placed on each newly silanized negative mold. The covered negative molds were then degassed in a vacuum desiccator for 25 minutes, and each mold was carefully flipped over onto plasma-cleaned, circular 25 mm diameter, #1 glass coverslips using curved tip tweezers. Next, mPADs were baked at 110°C for 20 hours. After being removed from the oven and cooled, mPADs were soaked in ethanol for 5 minutes and the negative molds were carefully removed with tweezers to prevent shearing of posts. mPADs were placed face down into another dish of ethanol and sonicated for 5 minutes to recover collapsed posts. They were supercritically dried (Samdri-PVT-3D; Tousimis) with liquid CO_2 to preserve post integrity.

Microcontact Printing and Cell Seeding

Flat slabs of PDMS were cut to the size of mPADs, sonicated in ethanol, and dried with a stream of N_2 .100 µL of a solution containing fibronectin (Gibco) (50 µg/mL) and Alexa Fluor 647 (AF647)-fibrinogen (Invitrogen) (27 µg/mL) was pipetted onto each stamp and left to incubate

for 1 hour at room temperature. During this incubation, the previously made mPADs were trimmed of excess PDMS to create a flat surface for stamping, then surface-oxidized for 10 minutes (UVO-Model 342; Jelight). After incubation, the fibronectin/fibrinogen-coated stamps were submerged in diH_2O and dried with a stream of N_2. The fibronectin/fibrinogen-coated surface was placed into contact with the surface of mPADs for 30 seconds, then stamps were removed in ethanol, and the inked mPADs were placed into PBS and moved into a tissue culture hood. mPADs were then passivated with 0.2% Pluronic F-127 solution for 1 hour at room temperature, which was replaced with PBS after the incubation with the Pluronic solution. Cells were counted and then seeded (40,000 cells/mPAD for MEFs and 20,000 cells/mPAD for hMSCs). Solution seeding (20,000 cells/mL for MEFs and 10,000 cells/mL for hMSCs) and 2 mL of cell suspension were used per device. Cells were seeded for 5 minutes at 37ºC and 5% CO_2 then unattached cells were aspirated away and the media was replaced with 2 mL of fresh media. This results in a cell density of 6000 cells/cm^2 for MEFs or 1600 cells/cm^2 for hMSCs for each device. Cells were left to spread overnight.

Imaging

Confocal microscopy with a Nikon C2 module connected to a Nikon Eclipse Ti inverted microscope or a Nikon W1 spinning disk confocal or a Nikon AX-R confocal microscope was used for live cell imaging. During imaging, cells were maintained in a stage incubator that controlled humidity, temperature, and CO_2 levels. Images were captured using high magnification objectives (60X Plan Apo VC Water Immersion objective, NA 1.2, Nikon; 100X Iris S Fluor Oil Immersion, NA 0.5-1.3, Nikon; 60X Plan Apo λD OFN25 DIC N2 Oil Immersion objective, NA 1.42, 100X Plan Apo λD OFN25 DIC N2 Oil Immersion objective, NA 1.45). Images of the top

surfaces of mPADs were captured using a 640 nm laser with a 685/50 nm filter, and images of eGFP-vinculin or cell tracker were captured using a 488 nm laser and 525/50 nm filter.

Force Measurement

Top surfaces of the microposts were labeled with AF647-fibrinogen to track their deflections. Microscopy images were acquired and deflections of micropost top surfaces were measured using a custom-made MATLAB macro (available upon request). Traction force, F, was calculated using the Bernoulli-Euler beam theory, in which E, D, L, and δ are the Young's modulus, post diameter, post height, and post deflection, respectively:

$$F = \delta \frac{3\pi E D^4}{64 L^3} \quad (\mathbf{1})$$

Below the parameters of mPADs used in this work are detailed:

- Post diameter (1.83 μm), center-center distance (4 μm), spring constant (22.30 nN/μm), effective modulus (17.21 kPa)
- Post diameter (0.80 μm), center-center distance (2 μm), spring constant (9.89 nN/μm), effective modulus (17.43 kPa)

Micropost Dimension Measurements

To confirm micropost dimensions, devices were surface-oxidized (UVO-Model 342; Jelight) for 10 minutes. The devices were then rehydrated by submersing them in separate dishes filled with the following solutions: (1) anhydrous ethanol, (2) 70% ethanol/30% water, (3) PBS, and (4) PBS. The samples were then put in a dry dish. The PBS droplet which was still covering the micropost area was mixed with a 100 μL droplet of PBS containing Alexa Fluor 647 (AF647)-fibrinogen (Invitrogen) (27 μg/mL). After mixing, 100 μL of the diluted fibrinogen solution was

then removed. Another 100 µL of PBS containing Alexa Fluor 647 (AF647)-fibrinogen (Invitrogen) (27 µg/mL) was added to the micropost area. The samples were incubated and covered for 1 hour at room temperature, washed once in PBS, and imaged. Images were captured using a 640 nm laser with a 685/50 nm filter and a 100X Plan Apo oil immersion objective (Table 1).

Adhesive Area Calculations

Since the microposts are arranged into a hexagonal lattice and the micropost tops are circular, a hexagonal packing arrangement was used. From equation 2, the packing density was calculated, where η is the packing density, A_h is the hexagon area, A_c is the micropost top area, D_h is the post center to center distance, and D_c is the diameter of a micropost top. From equation 3, the available adhesive area, A_a, is obtained from the packing density and the total adhesive area, A_t.

$$\eta = \frac{3A_c}{A_h} = \frac{\frac{3\pi}{4}{D_c}^2}{\frac{3\sqrt{3}}{2}{D_h}^2} \quad (\mathbf{2}) \qquad\qquad A_a = \eta A_t \quad (\mathbf{3})$$

Cell Area and Polarity Measurements

Cell area and polarity measurements were made in MATLAB. Cell area was calculated from a user drawn mask. The cell area mask was then fit to an ellipse which has the same normalized second central moment as the cell area mask. From this ellipse, the minor and major axis was determined and used to calculate the cell's polarity, using equation 4.

$$Polarity = \frac{Major\ Axis}{Minor\ Axis} \quad (\mathbf{4})$$

Statistical Analyses

Statistical analyses were performed using GraphPad Prism 8 (GraphPad Software Inc., La Jolla, CA). Statistical tests and P values are reported in the figure captions of the corresponding figures. To test for differences between groups, a two-sided unpaired t-test or its nonparametric equivalent was conducted. To examine the relationship between total traction force magnitude and cell spread area, a simple linear regression was conducted. Data is presented mean ± SD.

Article VII. Results and Discussion

mPADs are a powerful tool to measure lateral cellular traction forces. Each micropost provides independent and direct measurements of traction forces exerted by individual FAs formed on its top surface. However, mPADs restrict the size of FAs to the area of the post tops. While a variety of different mPAD configurations with different lattice structures, post dimensions, and post spacing have been used [8, 13-18], most studies focus on how micropost stiffnesses through changes in post height alter cellular functions. While changing the post top area will alter the post stiffness, it is usually done to increase post density and the spatial resolution of traction force measurements. Studies that investigate cell behavior on different post diameters are relatively few, and they have focused on the initial phases of cell adhesion [18] or endothelial adhesion patterns and cell spread area [13, 19]. Weng and Fu directly examined how microposts of different top areas but similar effective stiffnesses [20], a parameter that describes the effective Young's modulus of a micropost array [16], impact cell spread area and traction forces. In this study, we investigate whether micropost top area alters cell spread area and traction forces, in mouse embryonic fibroblasts and human mesenchymal stromal cells, when effective stiffness is kept constant.

We examined two different mPAD designs. (1) Micropost arrays with 0.50 μm^2 post top surface area (post diameter 0.80 μm) and a post center-to-center distance of 2 μm, and (2) micropost arrays with 2.63 μm^2 post top surface area (post diameter 1.83 μm) and a post center-to-center distance of 4 μm. Since it has been previously demonstrated that substrate rigidity alters cell contractility [21], we chose two mPAD designs that had compatible effective stiffnesses. For the 0.50 μm^2 post area mPADs, we used post heights of 2.48 μm to obtain an effective stiffness of 17.4 kPa. For the 2.63 μm^2 post area mPADs, we chose post heights of 5.70 μm to obtain an effective stiffness of 17.2 kPa (**Fig. 1**). MEFs expressing eGFP-vinculin were then seeded onto the mPADs, and after an overnight incubation, confocal microscopy images of MEFs were taken. Due to difficulties with imaging the 0.50 μm^2 post area mPADs, two different high magnification objectives were used: (1) a 60X water immersion objective and (2) a 100X oil immersion objective. For the 2.63 μm^2 post area mPADs, images were taken with the 60X water immersion objective, and for the 0.50 μm^2 post area mPADs, images were taken with the 100X oil immersion objective (**Fig. 2**). The post tops were labeled with AF647-fibrinogen and the cells expressed eGFP-vinculin. To confirm that there was not a difference in the captured accuracy of post deflections between the different objectives, we imaged the 2.63 μm^2 post area mPADs using both objectives and calculated the forces at individual FAs, and no differences were seen between the two objectives (**$p = 0.1868$, Fig. S1**). From these images, cellular area, morphology, and traction forces were extracted using a custom MATLAB macro, which generates an ideal grid based on user input to calculate post deflections and forces generated by the cell (**Fig. 3** and **Fig. 4**).

Cells were less spread on 0.50 μm^2 post area mPADs compared to those on the larger 2.63 μm^2 post area mPADs (**$p < 0.0001$, Fig. 4a**), and while they do adhere to a larger number of posts on the 0.50 μm^2 post area mPADs compared to those on the 2.63 μm^2 post area mPADs (**$p <$**

0.0001, Fig. 4b), this still results in less adhesive area presented to fibroblasts on the 0.50 μm^2 post area mPADs compared to the 2.63 μm^2 post area mPADs (**p < 0.0001, Fig. 4c**). These differences are likely due to the 2.63 μm^2 post area mPADs presenting a 30% larger available adhesive area when compared to the 0.50 μm^2 post area mPADs (**Fig. S2**). This difference in the available adhesive area may be a contributing factor to the extent to which fibroblasts spread. However, a previous study looking at microposts of similar dimensions but different post center-to-center distances show no difference in cell spread area, even though the available adhesive area changed by 65% [19]. This suggests that the difference in cell spread area seen in the present study is due to the difference in the micropost top surface area. Additionally, there was no difference in the polarity of fibroblasts between the two mPADs (**p = 0.9921, Fig. S3**). Notably, the observed trends in cell adhesion area between the mPAD configurations extended to cell-generated traction forces. Upon examining the force vector plots (**Fig. 3a**, **b**), it is evident that the micropost top surface area has an impact on cellular traction forces. Upon quantifying traction forces, cells generated higher total traction forces on the 2.63 μm^2 post area mPADs compared to the 0.50 μm^2 post area mPADs (**p < 0.0001, Fig. 4d**). Even when the cellular traction forces were normalized either to the number of adhered posts (**p < 0.0001, Fig. 4e**) or to the cell spread area (**p < 0.0001, Fig. 4f**), traction forces were still higher for mPADs with the larger post areas. This result is not surprising as linear correlations between traction force and cell area have been shown on micropost surfaces [10]. Interestingly, our results contrast with a prior study using NIH 3T3 fibroblasts. Instead of observing reductions in cell spread area and traction forces when post top area was reduced, Weng and Fu reported increases in cell spread area and traction forces [20]. An explanation for these contradictory findings is cell line-specific (NIH 3T3 cells vs. murine embryonic fibroblasts) differences in mechanoresponses and cell spreading.

To determine whether our findings were applicable to other mechanoresponsive cells, we repeated the experiments with human mesenchymal stromal cells (hMSCs). hMSCs are extensively used in mechanobiology studies as well as are under evaluation in numerous clinical trials. hMSCs attached on mPADs were imaged using a Nikon AX-R confocal system with the same 60X oil immersion objective (**Fig. 5**); low magnification images showing the distribution of individual cells on mPADs are provided in **Fig. S7**. For all metrics, results for hMSCs (**Fig. 6** and **Fig. S5**) mirrored the data obtained for MEFs. On the smaller micropost area (0.50 μm^2), hMSCs were less spread (**Fig. 6a**) and adhered to a larger number of posts (**Fig. 6b, c**) compared to the larger microposts (2.63 μm^2). Traction forces for hMSCs were lower on the smaller micropost areas compared to the larger microposts whether or not it was normalized via adhered posts or cell spread area (**Fig. 6d, e, f**). In terms of morphology, the hMSCs exhibited no differences in polarity when the micropost area was changed (**Fig. S5**). We note that a significant limitation of mPADs is the inability to measure out-of-plane forces, and the force component normal to the surface can in some instances approximate the lateral values [22]. Nevertheless, the analysis of the two cell types supports the conclusion that cell spreading area and increased focal adhesion area are the major drivers for increased traction forces on the larger area mPADs.

We next examined the relationship between traction force and cell spread area on both mPAD configurations. MEFs exhibited a linear relationship between total traction force magnitude and cell spread area regardless of the mPAD post top area (0.50 μm^2: **$p < 0.0001$, $R^2 = 0.6769$;** 2.63 μm^2: **$p < 0.0001$, $R^2 = 0.5828$, Fig. S4**), which agrees with previous findings for NIH 3T3 fibroblasts and HUVECs [20]. Further comparison into the regression line slopes showed no differences between the two different micropost areas (**$p = 0.1033$**, **Fig. S4**). The slope of the traction force-cell area relationship provides a useful metric to characterize cell contractility on

mPADs. Since substrate stiffness is a strong modulator of traction forces, the lack of differences in the traction force-cell area slope is not unexpected as both mPAD configurations had the same effective stiffness [21]. For hMSCs, a linear relationship between total traction force magnitude and cell spread area was again observed for both mPAD configurations (0.50 μm^2: **$p<0.0001$**, **$R^2 = 0.7816$;** 2.63 μm^2: **$p < 0.0001$, $R^2 = 0.7301$, Fig. S6**). For this cell type, however, there was a difference in the regression slopes **($p=0.005$**, **Fig. S6**). Cells on the 0.50 μm^2 post area devices exhibited a smaller regression slope than cells on the 2.63 μm^2 post area devices (0.414 $nN/\mu m^2$ vs. 0.845 $nN/\mu m^2$). We posit that the differences in regression slope for hMSCs reflect the high contractility and mechanosensitivity of these cells.

Article VIII. Conclusion

We show that reducing micropost top surface area while keeping post array effective stiffness constant results in decreased cell spread area and traction forces. In contrast, the traction force-cell area relationship maintained a linear dependence for different micropost top areas. This technical report highlights the impact of micropost top surface area on traction forces and cell spread area and supports the use of the slope of the traction force-cell area relationship as a metric to characterize cell contractility on elastic substrates.

Article IX. Acknowledgements

We acknowledge funding support from National Institutes of Health Award No. R01 EB024322.

Article X. Contributions

E.N.H and D.L. conducted experiments and analyses. A.J.G. conceptualized and supervised the research. J.F. provided mPAD master molds. E.N.H, D.L., and A.J.G. wrote and revised the manuscript.

Article XI. References

[1] T. Mammoto, A. Mammoto, and D. E. Ingber, "Mechanobiology and developmental control," *Annu Rev Cell Dev Biol,* vol. 29, pp. 27-61, 2013, doi: 10.1146/annurev-cellbio-101512-122340.

[2] J. Rosinczuk, J. Taradaj, R. Dymarek, and M. Sopel, "Mechanoregulation of Wound Healing and Skin Homeostasis," *Biomed Res Int,* vol. 2016, p. 3943481, 2016, doi: 10.1155/2016/3943481.

[3] W. J. Polacheck and C. S. Chen, "Measuring cell-generated forces: a guide to the available tools," *Nat Methods,* vol. 13, no. 5, pp. 415-23, Apr 28 2016, doi: 10.1038/nmeth.3834.

[4] D. W. Zhou and A. J. Garcia, "Measurement systems for cell adhesive forces," *J Biomech Eng,* vol. 137, no. 2, p. 020908, Feb 1 2015, doi: 10.1115/1.4029210.

[5] P. Roca-Cusachs, V. Conte, and X. Trepat, "Quantifying forces in cell biology," *Nat Cell Biol,* vol. 19, no. 7, pp. 742-751, Jul 2017, doi: 10.1038/ncb3564.

[6] A. J. Garcia, P. Ducheyne, and D. Boettiger, "Quantification of cell adhesion using a spinning disc device and application to surface-reactive materials," *Biomaterials,* vol. 18, no. 16, pp. 1091-1098, 1997, doi: 10.1016/S0142-9612(97)00042-2.

[7] Y. Liu, K. Galior, V. P. Ma, and K. Salaita, "Molecular Tension Probes for Imaging Forces at the Cell Surface," *Acc Chem Res,* vol. 50, no. 12, pp. 2915-2924, Dec 19 2017, doi: 10.1021/acs.accounts.7b00305.

[8] J. L. Tan, J. Tien, D. M. Pirone, D. S. Gray, K. Bhadriraju, and C. S. Chen, "Cells lying on a bed of microneedles: an approach to isolate mechanical force," *Proc Natl Acad Sci U S A,* vol. 100, no. 4, pp. 1484-9, Feb 18 2003, doi: 10.1073/pnas.0235407100.

[9] M. T. Yang, J. Fu, Y. K. Wang, R. A. Desai, and C. S. Chen, "Assaying stem cell mechanobiology on microfabricated elastomeric substrates with geometrically modulated rigidity," *Nat Protoc,* vol. 6, no. 2, pp. 187-213, Feb 2011, doi: 10.1038/nprot.2010.189.

[10] D. W. Dumbauld *et al.*, "How vinculin regulates force transmission," *Proc Natl Acad Sci U S A,* vol. 110, no. 24, pp. 9788-93, Jun 11 2013, doi: 10.1073/pnas.1216209110.

[11] J. Galipeau *et al.*, "International Society for Cellular Therapy perspective on immune functional assays for mesenchymal stromal cells as potency release criterion for advanced phase clinical trials," (in English), *Cytotherapy,* vol. 18, no. 2, pp. 151-159, Feb 2016, doi: 10.1016/j.jcyt.2015.11.008.

[12] J. Fu *et al.*, "Mechanical regulation of cell function with geometrically modulated elastomeric substrates," *Nat Methods,* vol. 7, no. 9, pp. 733-6, Sep 2010, doi: 10.1038/nmeth.1487.

[13] L. E. Dickinson, D. R. Rand, J. Tsao, W. Eberle, and S. Gerecht, "Endothelial cell responses to micropillar substrates of varying dimensions and stiffness," *J Biomed Mater Res A,* vol. 100, no. 6, pp. 1457-66, Jun 2012, doi: 10.1002/jbm.a.34059.

[14] O. du Roure *et al.*, "Force mapping in epithelial cell migration," *Proc Natl Acad Sci U S A,* vol. 102, no. 7, pp. 2390-5, Feb 15 2005, doi: 10.1073/pnas.0408482102.

[15] M. Gupta *et al.*, "Adaptive rheology and ordering of cell cytoskeleton govern matrix rigidity sensing," *Nat Commun,* vol. 6, p. 7525, Jun 25 2015, doi: 10.1038/ncomms8525.

[16] M. Ghibaudo *et al.*, "Traction forces and rigidity sensing regulate cell functions," (in English), *Soft Matter,* vol. 4, no. 9, pp. 1836-1843, 2008, doi: 10.1039/b804103b.

[17] J. A. VanderBurgh, H. Hotchkiss, A. Potharazu, P. V. Taufalele, and C. A. Reinhart-King, "Substrate stiffness heterogeneities disrupt endothelial barrier integrity in a micropillar model of heterogeneous vascular stiffening," *Integr Biol (Camb),* vol. 10, no. 12, pp. 734-746, Dec 19 2018, doi: 10.1039/c8ib00124c.

[18] S. Ghassemi *et al.*, "Cells test substrate rigidity by local contractions on submicrometer pillars," *Proc Natl Acad Sci U S A,* vol. 109, no. 14, pp. 5328-33, Apr 3 2012, doi: 10.1073/pnas.1119886109.

[19] M. T. Yang, N. J. Sniadecki, and C. S. Chen, "Geometric considerations of micro- to nanoscale elastomeric post arrays to study cellular traction forces," (in English), *Adv Mater,* vol. 19, no. 20, pp. 3119-+, Oct 19 2007, doi: 10.1002/adma.200701956.

[20] S. Weng and J. Fu, "Synergistic regulation of cell function by matrix rigidity and adhesive pattern," *Biomaterials,* vol. 32, no. 36, pp. 9584-93, Dec 2011, doi: 10.1016/j.biomaterials.2011.09.006.

[21] J. P. Califano and C. A. Reinhart-King, "Substrate Stiffness and Cell Area Predict Cellular Traction Stresses in Single Cells and Cells in Contact," *Cell Mol Bioeng,* vol. 3, no. 1, pp. 68-75, Mar 1 2010, doi: 10.1007/s12195-010-0102-6.

[22] W. R. Legant *et al.*, "Multidimensional traction force microscopy reveals out-of-plane rotational moments about focal adhesions," (in English), *P Natl Acad Sci USA,* vol. 110, no. 3, pp. 881-886, Jan 15 2013, doi: 10.1073/pnas.1207997110.

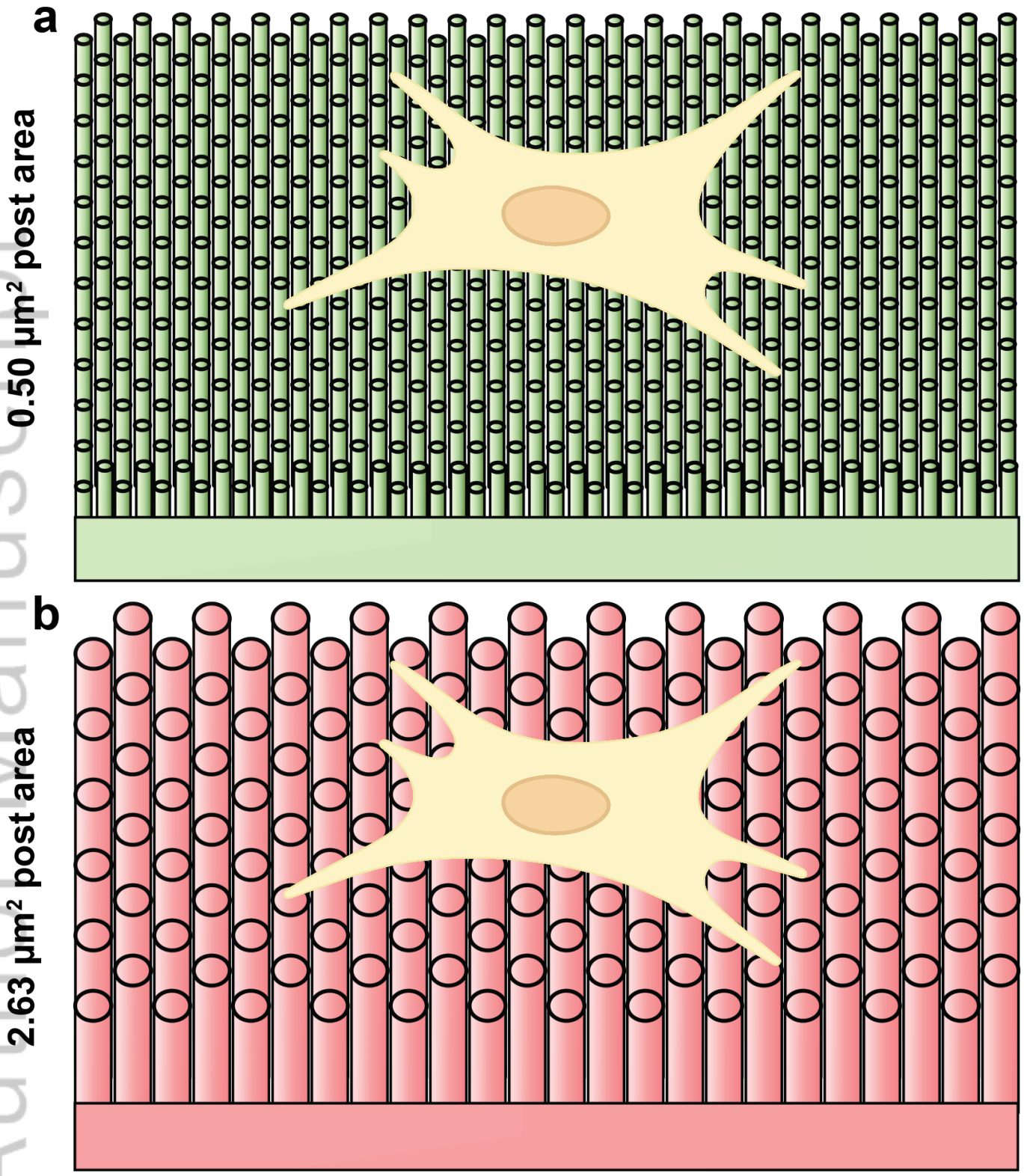

Figure 1. 3D Diagrams of MEFs Seeded on Micropost Arrays. (**a**) 0.80 μm diameter posts (0.50 μm^2 post area) and 2.48 μm height. (**b**) 1.83 μm diameter posts (2.63 μm^2 post area) and 5.70 μm height. Diagrams are proportional to each other.

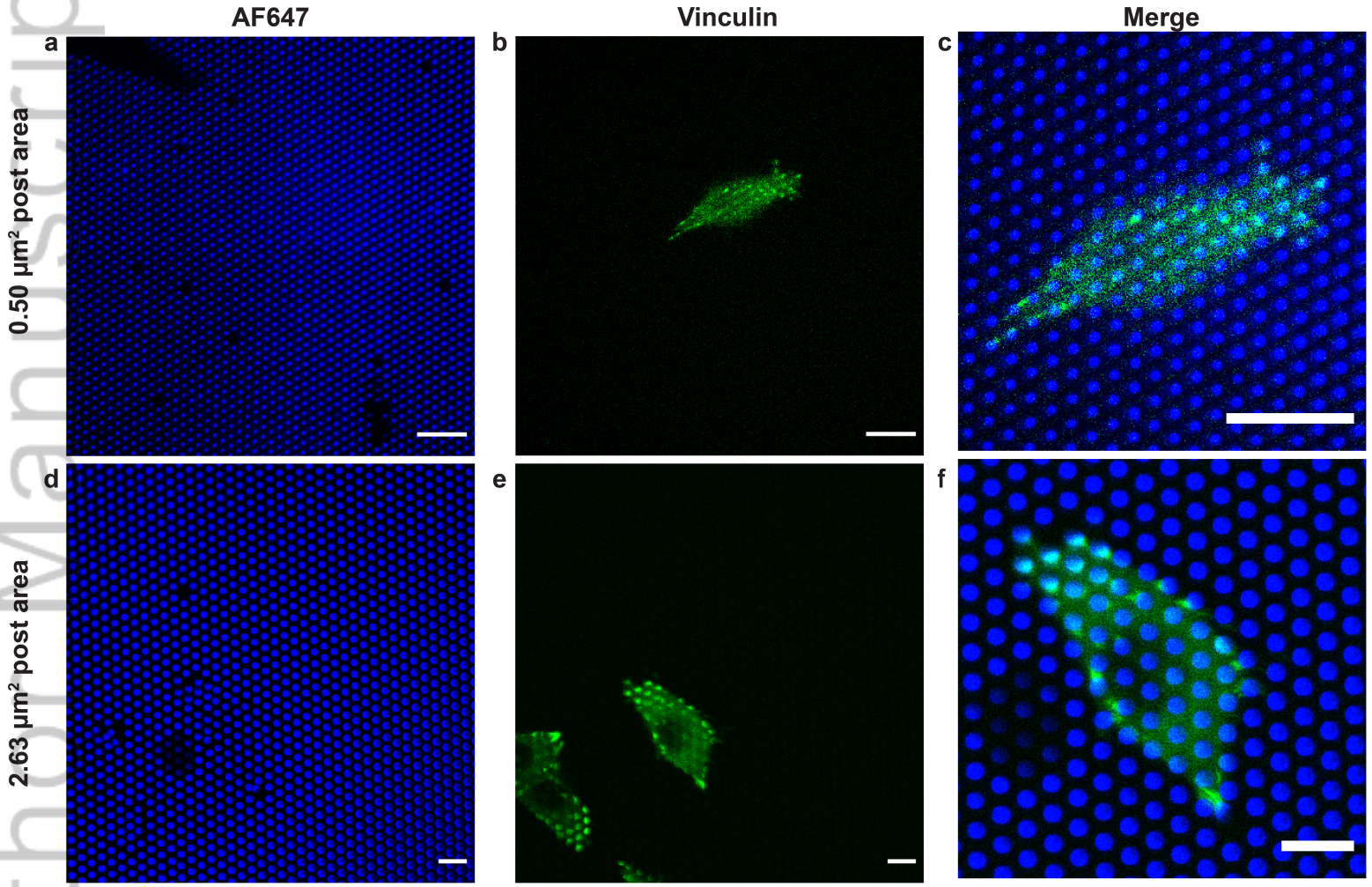

Figure 2. Confocal Microscopy Representative Images. (**a**) 0.50 μm² post area mPAD image with 100X objective. (**b**) eGFP-Vinculin for MEF on 0.50 μm² post area mPAD with 100X objective. (**c**) Merge image of the post and vinculin images on 0.50 μm² post area mPAD with 100X objective. (**d**) 2.63 μm² post area mPAD image with 60X objective. (**e**) eGFP-Vinculin for MEF on 2.63 μm² post area mPAD with 60X objective. (**f**) Merge image of the post and vinculin images on 2.63 μm² post area mPAD with 60X objective. Scale bar 10 μm.

JBMA_37518_Figure-2 DP-Checked-012623.png

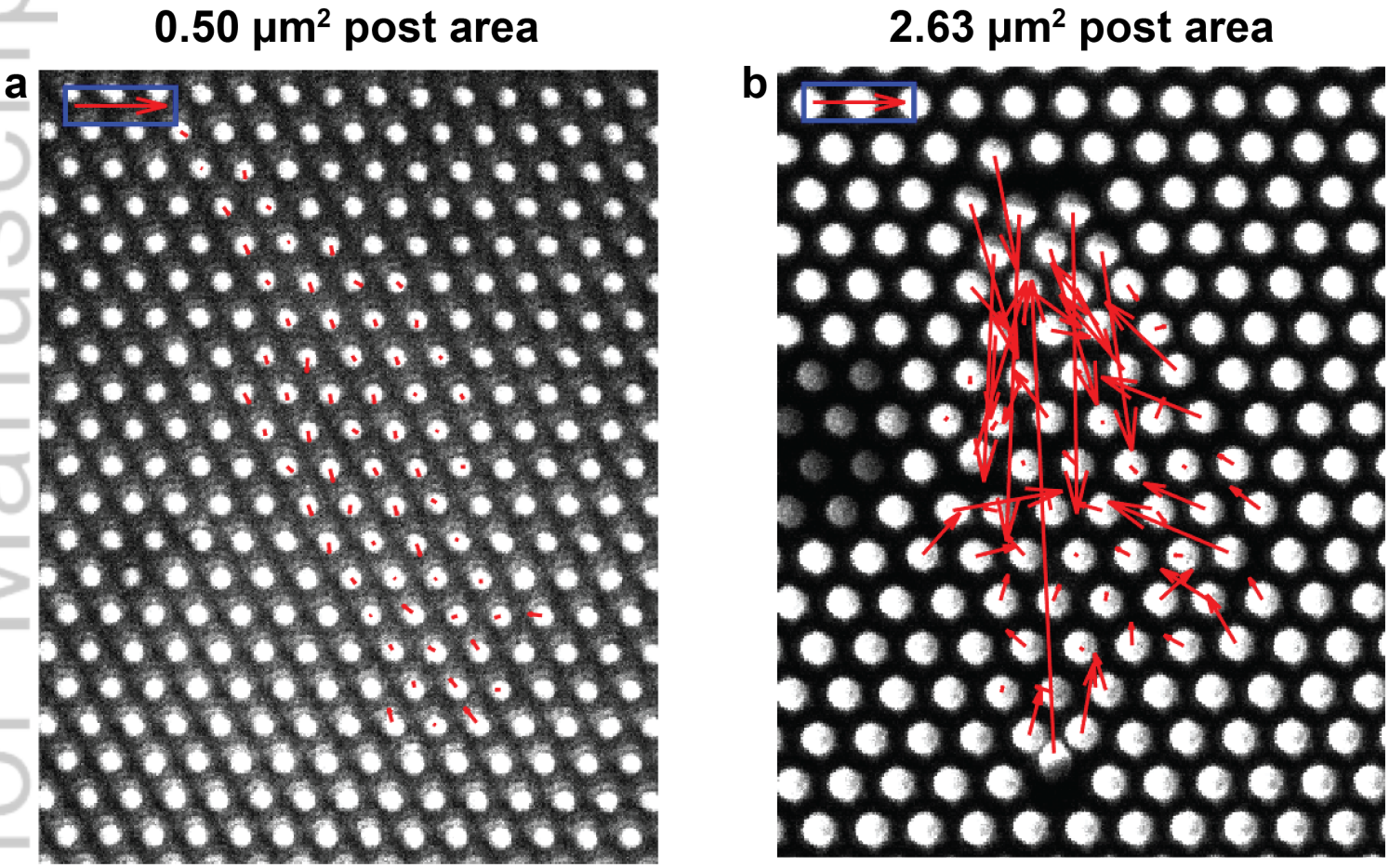

Figure 3. Force Vector Maps for MEFs. (**a**) MEF exerting force on 0.50 μm² post area mPAD. (**b**) MEF exerting force on 2.63 μm² post area mPAD. The arrow inside the blue blox represents a scaling arrow of 10 nN.

JBMA_37518_Figure-3-DP-Checked-012023.png

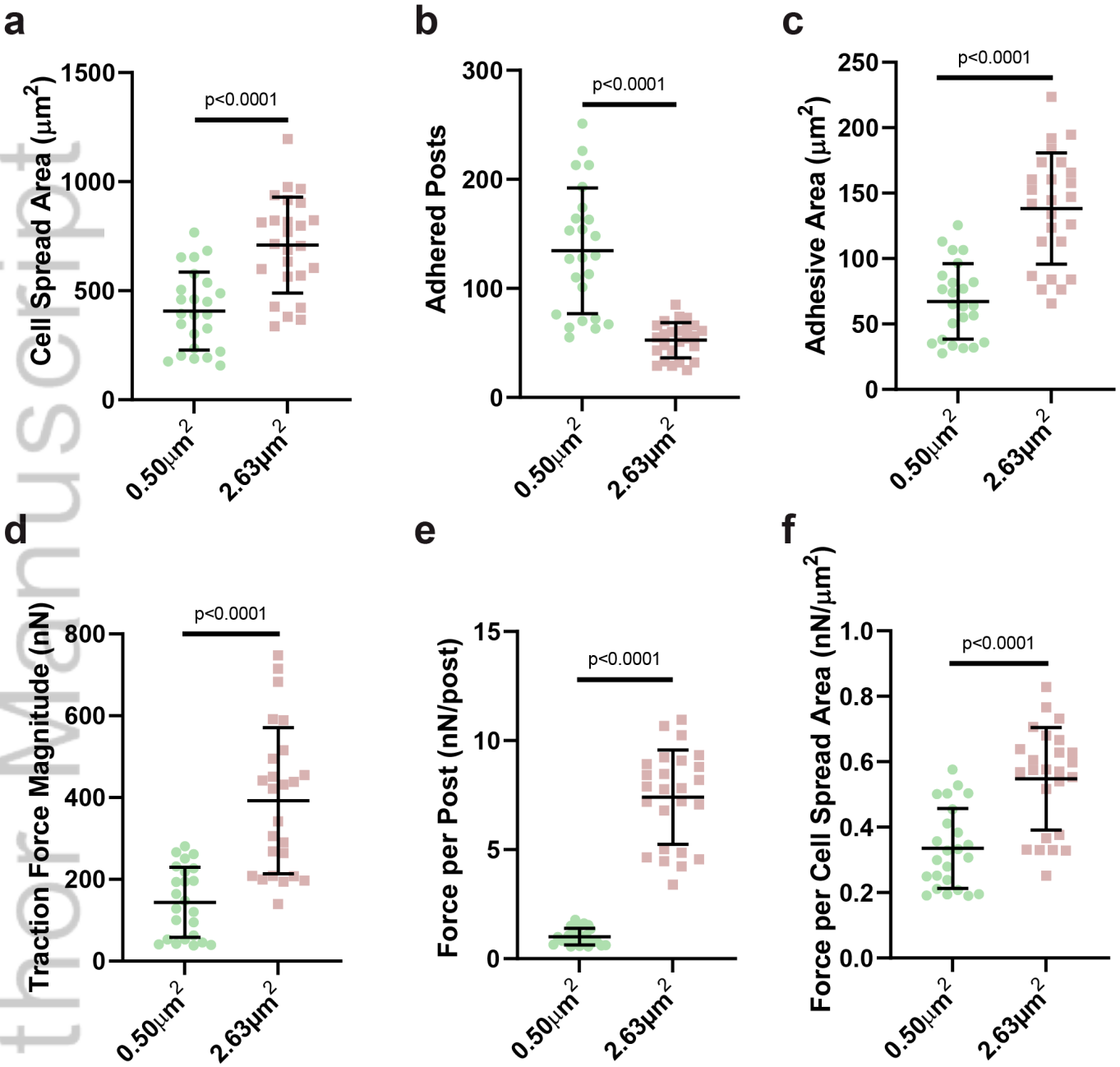

Figure 4. Post Area Influence on MEF Mechanoresponses. (a) Cell Spread Area (mean ± SD). Two-sided unpaired t-test p<0.0001. (**b**) Total number of adhered posts (mean ± SD). Two-sided t-test with Welch's correction factor p<0.0001. (**c**) Adhesive Area (mean ± SD) Two-sided unpaired t-test p<0.0001. (**d**) Traction Force Magnitude (mean ± SD). Two-sided t-test with Welch's correction factor p<0.0001. (**e**) Force per Post (mean ± SD). Two-sided t-test with Welch's correction factor p<0.0001. (**f**) Force per Cell Spread Area (mean ± SD). Two-sided unpaired t-test p<0.0001. n=24 for the 0.50μm² and n=25 for the 2.63μm² conditions.

JBMA_37518_Figure-4 DP-Checked-01262023.png

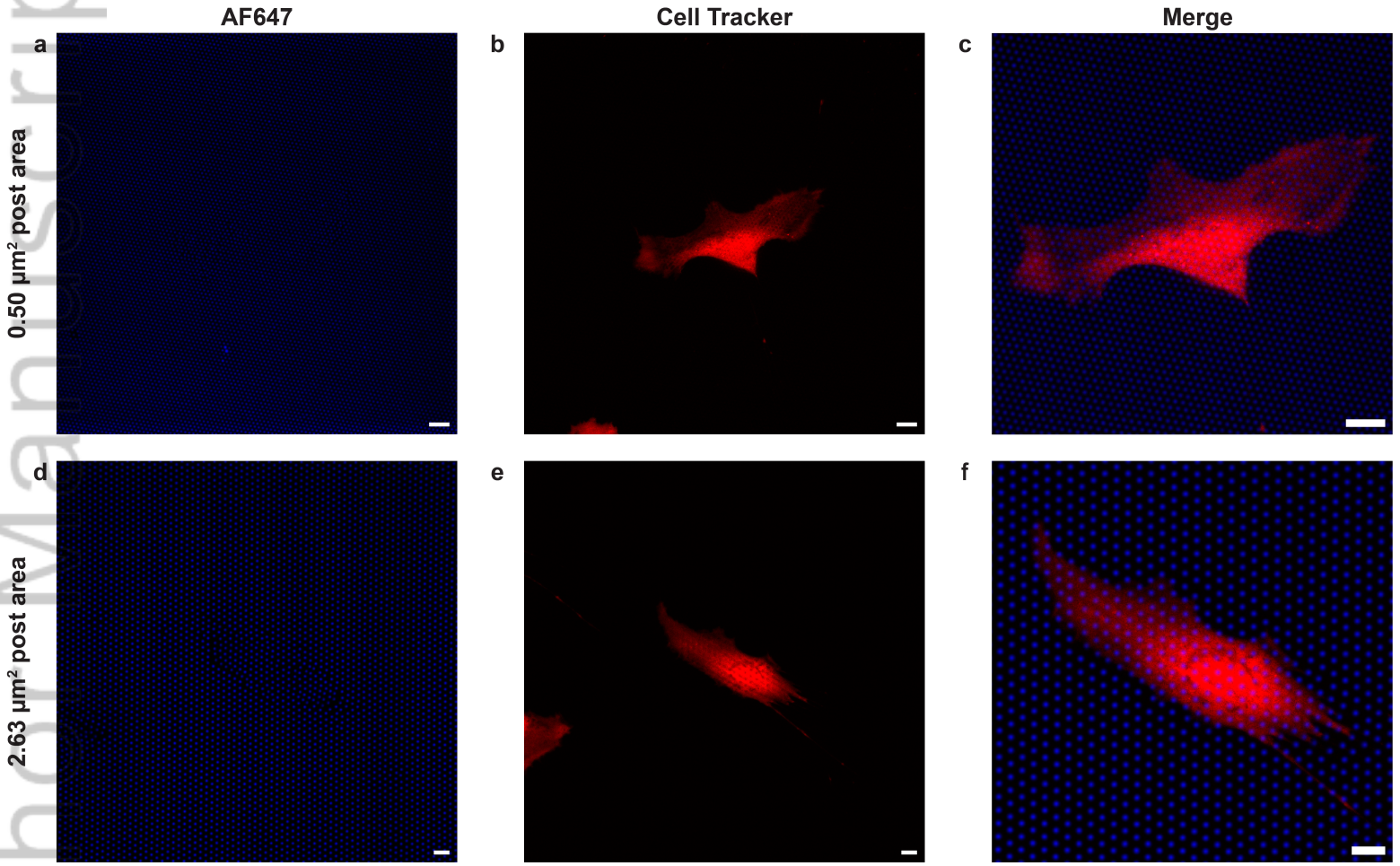

Figure 5. Confocal Microscopy Representative Images. (**a**) Mini (0.50 μm² post area) post image. (**b**) Cell tracker image of hMSC on 0.50 μm² post area mPAD. (**c**) Merge image of the post and cell tracker images on 0.50 μm² post area mPAD. (**d**) Regular (2.63 μm² post area) post image. (**e**) Cell tracker image of hMSC on 2.63 μm² post area mPAD. (**f**) Merge image of the post and cell tracker images on 2.63 μm² post area mPAD. Scale bar 10 μm.

JBMA_37518_Figure-5-DP-Checked-01262023.png

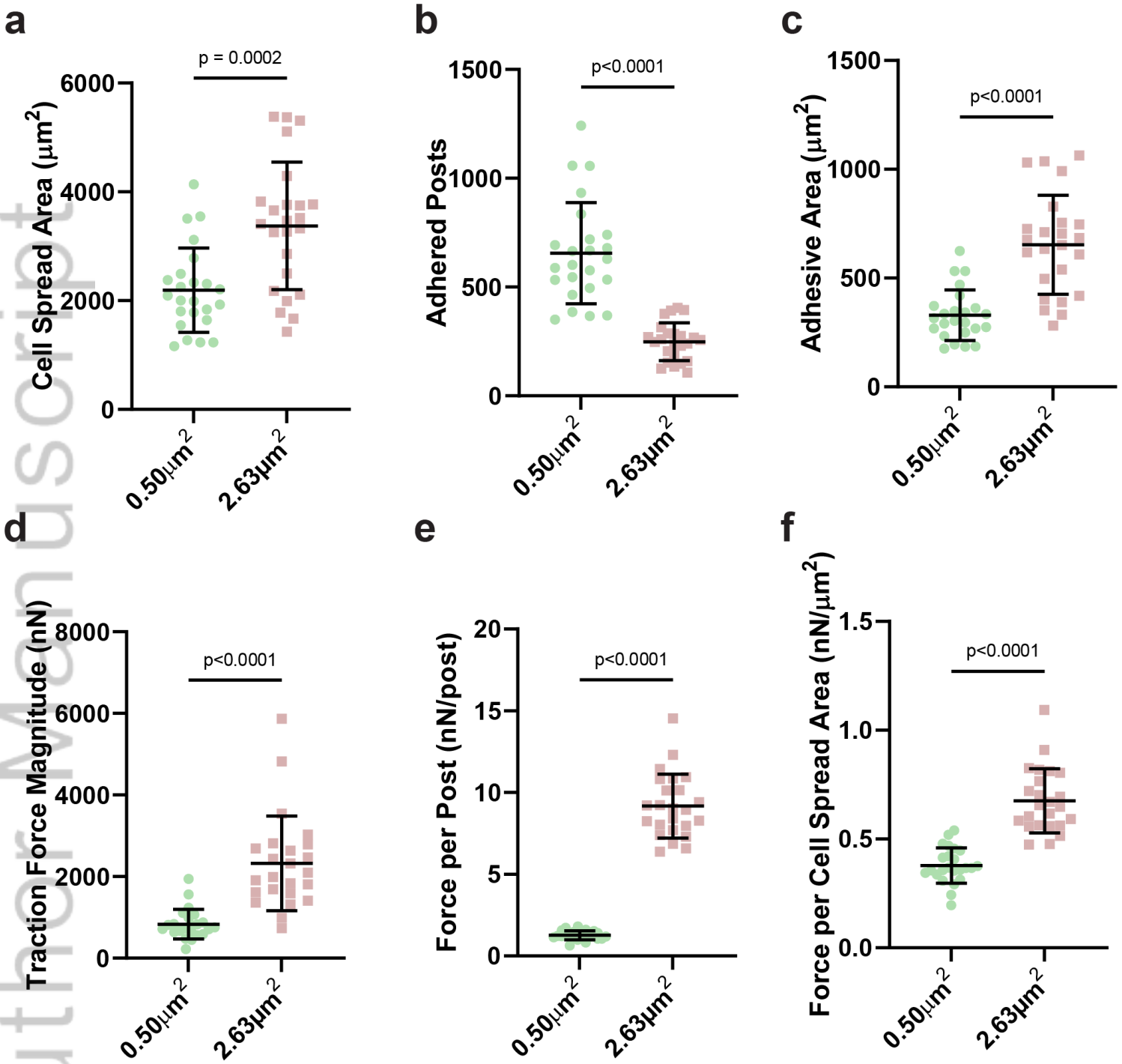

Figure 6. Post Area Influence on hMSC Mechanoresponses. (a) Cell spread area (mean ± SD). Two-sided unpaired t-test p=0.0002. (**b**) Total number of adhered posts (mean ± SD). Two-sided t-test with Welch's correction factor p<0.0001. (**c**) Adhesive Area (mean ± SD) Two-sided t-test with Welch's correction factor p<0.0001. (**d**) Traction Force Magnitude (mean ± SD). Mann-Whitney test p<0.0001. (**e**) Force per Post (mean ± SD). Two-sided t-test with Welch's correction factor p<0.0001. (**f**) Force per Cell Spread Area (mean± SD). Two-sided t-test with Welch's correction factor p<0.0001. n=24 for the 0.50μm² and n=24 for the 2.63μm² conditions.

JBMA_37518_Figure-6-DP-Checked-01262023.png

Micropost Area	Predicted Post Diameter	Measured Post Diameter (Mean ± SD)	Predicted Post Height	Measured Post Height (Mean ± SD)
0.50 μm^2	0.80 μm	0.78 ± 0.04 μm	2.48 μm	2.46 ± 0.14 μm
2.63 μm^2	1.83 μm	1.85 ± 0.03 μm	5.70 μm	5.73 ± 0.14 μm

Table 1. Fabrication parameters for mPADs.